Materials and Design 91 (2016) 424–431

Contents lists available at ScienceDirect

Materials and Design

journal homepage: www.elsevier.com/locate/matdes

Visualisation of alternating shielding gas flow in GTAW

I. Bitharas [a,*], S.W. Campbell [b], A.M. Galloway [b], N.A. McPherson [b], A.J. Moore [a]

[a] Institute of Photonics and Quantum Sciences, Heriot-Watt University, Edinburgh EH14 4AS, UK
[b] Department of Mechanical and Aerospace Engineering, University of Strathclyde, Glasgow G1 1XQ, UK

ARTICLE INFO

Article history:
Received 11 August 2015
Received in revised form 13 November 2015
Accepted 24 November 2015
Available online 2 December 2015

Keywords:
GTAW
Alternating
Shielding
Gases
Schlieren
Visualisation

ABSTRACT

The alternating shielding gas technique is a method of achieving transient arc characteristics during arc welding; however the complex flow that occurs through its use has not been investigated previously. A schlieren system was used to image density gradients that arise when alternating argon and helium shield gases, under varying flow parameters, with gas tungsten arc welding (GTAW). A theoretical analysis was carried out to determine the conditions under which the technique facilitates arc pulsing, in particular to avoid mixing of the shield gases in the delivery pipe prior to the welding nozzle. At appropriate pulsing frequency and flow rates, a stable horizontal region of helium was observed in the weld region, maintained in position by the denser argon from the preceding pulse. This higher than average mass fraction of helium when applying the shielding gases alternately, compared to a premixed gas with the same volume of argon and helium, increased the weld penetration by 13% on average, suggesting a modest improvement in heat transfer.

1. Introduction

Shielding gases are a fundamental component of several arc welding processes. Their primary functions are to protect the metal transfer stream and molten weld pool from contamination by atmospheric gases and to provide a medium for the electrical current to flow in the plasma jet between workpiece and electrode. Although the standard inert gas for any shielding application is pure argon, a variety of argon-based gas mixtures are used in industrial practice. By adding gases such as helium carbon dioxide or oxygen, the thermophysical properties of the plasma are controlled, resulting in numerous improvements in heat transfer, arc formation, gas coverage or material weldability.

Pulsing the shielding gas to achieve dynamic in-process changes to arc power was first proposed in 1967 for welding and cutting [1] in which pulses of a second shield gas, such as helium, were incorporated into the main argon flow via a modified torch design. Subsequently, a valve-regulated gas delivery system that alternated the shielding gases in the same feed line to the welding nozzle was used for the same purpose in [2]. Variations in the arc conductivity were noted, and it was suggested that these produced a higher total power and caused a varying pressure and effective diameter of the arc. The pulsed gas delivery method has been used in both gas metal arc welding (GMAW) and gas tungsten arc welding (GTAW) of aluminium alloys [2–4], as well as of carbon [5–7] and stainless [8,9] steels. Several benefits were reported, such as improved distortion control and re-work reduction [7,10] or refinement of weld structure and thus better mechanical the mechanical properties of the weld [2,8]. The pulsing frequency was shown to influence the dynamics of the melt pool [9] and final geometry of the solidified weld [8,10].

Such results therefore imply the potential for an increase in productivity or shielding gas efficiency due to improved heat and momentum transfer towards the weld pool. However, the uptake of the process has been slow because the economic and technical benefits claimed are based on mechanisms which have not been completely understood and quantified. The effect of gas mixing and pre-mixing on the shielding gas flow have not been analysed, and no imaging of the shielding gas flow has been reported.

In this paper, we demonstrate that alternating argon and helium shielding gas flows can be visualised effectively during GTAW with high-speed schlieren imaging. The effect that changes in the pulsing frequency and flow rate have on the flow and arc characteristics are analyzed, and contrasted with imaging sequences of pure and premixed flows. Also, the effect of pre-mixing of the shielding gases in the delivery pipe to the welding nozzle is established analytically through axial dispersion calculations. It is shown that low pulse rates and high flow rates make more efficient use of the helium, because it is held in the weld region by the denser argon from the preceding pulse, whereas high pulse rates and low flow rates result in the shielding gases being delivered premixed. Macrographs of the weld section show that alternating the gases increased weld penetration by 13% on average compared to using them pre-mixed.

* Corresponding author.
E-mail address: ioannisbitharas@gmail.com (I. Bitharas).

http://dx.doi.org/10.1016/j.matdes.2015.11.085

2. Flow visualisation during arc welding

Flow visualisation techniques have been used to observe shielding gas flow in GMAW and GTAW [11–17]. In particular, shadowgraphy and schlieren techniques enable localised refractive index gradients to be visualised. These gradients arise in welding due to large temperature and pressure gradients associated with the magnetohydrodynamic (MHD) flow and in regions where the shielding gas meets and mixes with the environment.

Gibson [12] measured the shielding gas coverage using aluminium and titanium GTAW spot welds for various weld conditions, including shielding gas composition, stand-off distance and cross draughts. It was shown that reducing the stand-off distance improves the shielding quality and that while nozzle size affects the coverage, a simple relationship between nozzle diameter, standoff and coverage was not determined. Of particular relevance to this study, it was found that half as much volume of argon was required as helium to achieve the same effective coverage. It was also observed that the flow of argon became turbulent at flow rates considerably lower than for helium, while an 80% argon/20% helium mixture became turbulent at a flow rate midway between the two and achieved increased weld penetration with respect to 100% argon gas.

Okada et al. [13] implemented a combination of shadowgraphy and chromatography in order to visualise the shielding gas flow with a laser source while measuring the shielding gas concentration in the arc region. The boundary of the laminar flow area visualised by shadowgraphy directly below the nozzle was found to coincide with 90–99% lines of equi-concentration of the argon shielding gas measured by gas chromatography. Regions visualised at the flow's edges also corresponded principally to concentration gradients.

In order to visualise the alternating shielding gas flow, we constructed a schlieren system. Fig. 1 shows a schematic of the optical setup that used Toepler's double parabolic mirror arrangement in order to minimise optical aberrations [18]. Two 100 mm diameter, parabolic field mirrors with a focal length of 1.27 m, M1 and M2, were located approximately two focal lengths apart. Aligned in a Z-type arrangement, M1 collimated the light from the light-emitting diode (LED) source while M2 focused it to a spot. Ideally the included 'Z' angles should be less than 3° in order to reduce the separation of the tangential and sagittal focus planes of M2. However, in order to incorporate the welding torch between the mirrors, while keeping the distance between the mirrors within the confines of the welding bay, it was necessary to increase the 'Z' angles of the mirrors to approximately 8°. The result was a small amount of astigmatism in the recorded images.

The light source was a 10,000 lm warm white LED, with an intensity spectrum peaking at approximately 630 nm. The light was collected by two condenser lenses, L1 and L2, with focal lengths of 120 mm and 60 mm respectively, in a telescope arrangement to reduce the LED's spot size at the source slit and to maximise the light collection efficiency. The shape and size of the source slit determines the sensitivity and measurement range of the schlieren system [19]. We used a 2 mm × 6 mm rectangular source slit with the long edge vertical, as recommended by Siewert et al. for welding applications [17]. The source slit was positioned at the focus of M1, to produce an image of the source at the focus of M2.

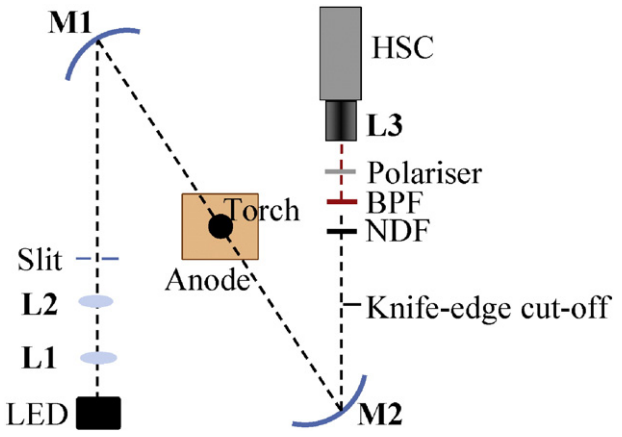

Fig. 1. Schematic of Z-type schlieren and alternating gas GTAW setup. The optical system comprised a high intensity light emitting diode (LED) source, parabolic mirrors, a combination of filters and a high-speed camera (HSC).

In order to match the source slit, a vertical knife-edge cut-off was positioned midway between the tangential and sagittal focal (Fourier) planes of M2 using a micrometre precision XY stage. The knife-edge filtered the refracted light so that the image formed by the high-speed camera (HSC) represented the change in intensity proportional to the gradient of the refractive index $\partial n/\partial x$ which in turn is proportional to the density gradient $\partial \rho/\partial x$, [19], where the x-direction is taken to be horizontal. In order to achieve a uniform measurement range, 50% of the image of the source slit was blocked by the knife-edge filter.

Images were recorded at a resolution of 256 × 256 pixels using a Kodak Ektapro high-speed camera, with a variable focus macro lens (L3). The exposure time was varied based on the level of radiation from the object by adjusting the frame-rate of the camera. Gas flows without welding were imaged at 4500 frames per second (fps) and there was no need for additional optical filters between the knife-edge cut-off filter and the high-speed camera. For GTAW welding, filters were added between the knife-edge and the camera in order to reduce the bright light emitted from the plasma. Spectroscopic analyses of GTAW argon arcs for copper have shown that no peaks in intensity are present in the region around 630 nm [20]. Thus a 633 nm ± 10 nm full-width-half-maximum band-pass filter (BPF) was used to eliminate as much arc light as possible. Narrower band pass filters at 633 ± 1 nm and ±3 nm were also tested but reduced the source light to a level below the sensitivity of the camera. A polariser was used to remove glare from the workpiece. Finally a neutral density filter (NDF) was included and the high-speed camera frame rate was reduced to 750 fps to record images.

3. GTAW experimental setup

The welding study was conducted using a stationary welding torch located between the mirrors M1 and M2 with the arc struck on to a water-cooled copper plate to prevent melting of the anode surface. A 2.4 mm diameter, 2% thoriated tungsten electrode was used throughout, with a 45° vertex angle. A 12.2 mm internal diameter nozzle with a 5 mm stand-off distance was used to direct the shielding gas flow.

In order to alternate the shield gas flow, a dedicated electronic gas control unit was designed, allowing the two shielding gas supplies to be connected to the welding torch. The unit utilises two timing circuits, which regulate the flow of each gas independently by giving a control signal to a solenoid valve on each gas line. The volumetric flow rate of both gases was set to be equal but supplied to the main hose at inverse time intervals of equal duration within the period of one shielding gas switching cycle, i.e. a 50% duty cycle between the two gases. A schematic diagram of the shielding gas control system is shown in Fig. 2.

In order to maintain consistency in the results, all trials were performed using DC electrode negative with a constant welding current of 100 A. However, due to the difference in their ionisation potentials, a higher arc voltage was required to maintain an arc for helium (~19 V) than for argon (~13 V), resulting in lower total power for argon. Welds were carried out using the pure gases to establish the upper and lower bounds of the available heat input. When alternating the shield gases, the current was again held constant at 100 A and the voltage was observed on the welding power supply to fluctuate at the pulsing frequency between these extremes, according to the shield gas composition and flow conditions. Such fluctuations in voltage are well-known in alternating shielding gas flows with GTAW and typical

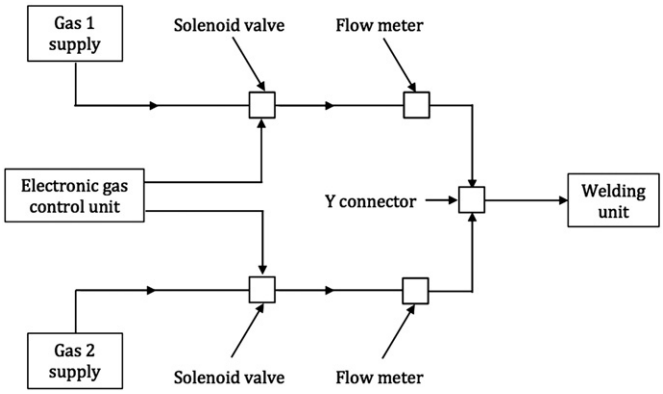

Fig. 2. Schematic diagram of the control system used for alternating the shield gases. The argon and helium gas cylinders were connected to the welding torch through solenoid valves, controlling the gas cycling over time.

waveforms are shown in [8]. Therefore, the amount of energy put into a given weld is associated with how efficiently the available helium is utilised, and the effect of varying flow conditions on the resulting welds was thus directly comparable by keeping the volumetric mass fractions constant.

4. Results

In order to analyse the motion and identify the ambient properties of the gases used during the GTAW process, 'cold' flow imaging of the shielding gas flow without an arc was carried out to supplement 'hot' flows where the arc plasma was present. To provide a comprehensive reference, flow rates of 5 and 10 l/min for argon, helium, and alternating shielding gases at frequencies of 2 and 8 Hz were imaged.

4.1. Pure argon

The flow visualisations of argon are shown in Fig. 3. The difference in refractive index between the surrounding air and the shielding gas determines the amount of refraction and hence the visibility of flow features [13,19]. Analysis of the light passing through an idealised gas column at the same temperature as the surrounding air shows that argon refracts by an order of magnitude less than helium [13,21]. Therefore the visualisation of the 'cold' argon flow showed weak refractive index gradients and rather poor visibility in the schlieren image. The schlieren sensitivity was increased for the 'cold' argon flow only by reducing the slit width to 3.2 mm; fluid motion and mixing of argon with air is just discernible in Fig. 3, although it was more observable in the high-speed video sequences. A laminar stream of argon exits the welding nozzle and spreads out over the workpiece surface due to its higher density than air, preventing environmental contamination near the weld bead. In the radial direction, the flow was mildly turbulent for the 10 l/min case with eddies forming away from the weld region, where the gas mixed with the surrounding air. It should be noted that the three distinct vertical, black lines (one just to the left of the tungsten electrode, one beneath and the other just to the right of the nozzle) are due to mirror scratches. These mirror defects can be seen in all subsequent images to some degree.

Fig. 3 also shows the case for the 'hot' argon visualisations recorded during GTAW welding. The intense self-luminance of the argon plasma was brighter than the source despite the band pass filter, obscuring any axial flow features immediately below the tungsten electrode. However, the heated shielding gas increased the refractive index gradients elsewhere in the image enabling two distinct flow features to be seen in the figure. The first feature is a bell-shaped density gradient around the arc that was not visible in the 'cold' flow. This feature is characteristic of the downwards plasma jet: resistive, thermoelectric and thermionic heating cause the dissociation of gas particles which are accelerated due to Lorentz forces in the inter-electrode region [22,23]. The second feature in the images is the bulk flow of the shielding gas, closer to the nozzle edges, which does not interact heavily with the arc. Within this secondary jet, momentum is transferred only under the influence of gravity and viscous stresses, and the mean velocity is much lower than that of the plasma flow [22]. The form of this feature is similar to that seen on the 'cold' flow images, including mixing at the interface with the environment. Buoyant mixing occurs at the boundary with the surrounding air as the heated argon rises up due to its reduced density and mixes with air. At 5 l/min there was a strong horizontal density gradient, suggesting a local equilibrium in concentrations at the argon–air interphase. At 10 l/min, the mixing became more turbulent and no steady-state density gradient was observed.

4.2. Pure helium

The use of pure helium as a shielding gas in GTAW is not a common choice, mainly due to the prohibitive cost but also because arc initiation is harder and arc stability is limited [11]. However, in order to establish a benchmark of its characteristics, its flow was visualised as shown in Fig. 4. The nozzle has been delineated in the first frame to distinguish it from a large dark region in the schlieren image. The net emission coefficient of helium is an order of magnitude lower than that of argon [24]. Therefore, in the 'hot' flow visualisations for helium, light from

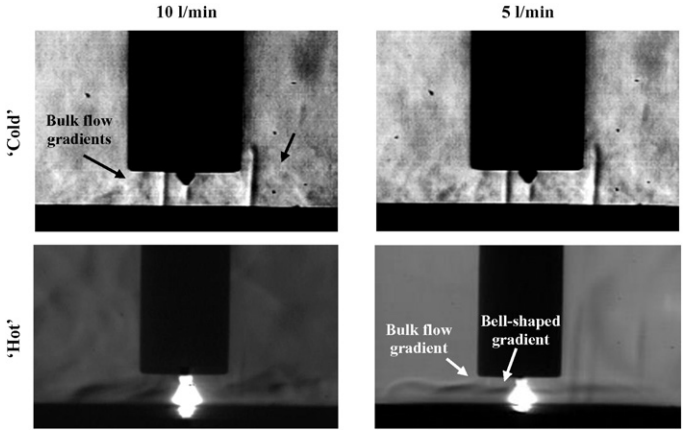

Fig. 3. Steady state schlieren images of argon gas flows showing density gradients observed during 'cold' and 'hot' flows. The three vertical black lines in the 'cold' images are due to scratches in the parabolic mirrors, as discussed in the text.

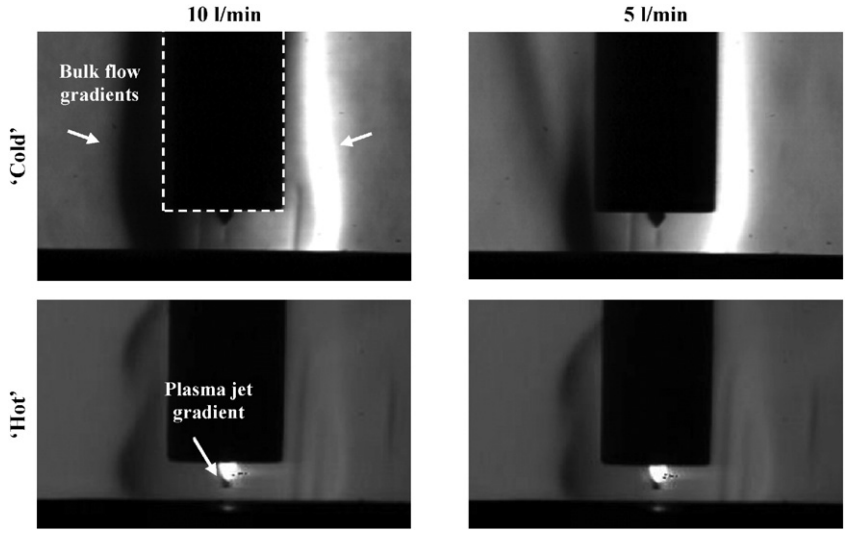

Fig. 4. Steady state schlieren images of helium gas flows showing density gradients observed during 'cold' and 'hot' flows.

the bell-shaped plasma beneath the tungsten electrode was eliminated by the band pass and neutral density filters.

The 'cold' visualisations for helium show a smoother flow than those for argon. The bulk flow gradients show buoyancy forces carry the gas upwards, creating a 'bulb' shaped plume, as internal viscous forces quickly eliminate any vortices and a steady state flow is reached. Comparison of the steady state flows between 5 and 10 l/min showed that the coverage on the workpiece was increased in diameter when using the higher flow rate.

In the 'hot' images of Fig. 4, a short cylindrical refractive index gradient feature can be seen immediately below the electrode due to the plasma jet. This cylindrical feature does not extend fully to the anode and extends only slightly beyond the electrode, suggesting that a body force is acting heavily on the flow close to the anode. Based on numerical magneto-hydrodynamic models [24–27], the plasma jet is indeed expected to decelerate, as the axial Lorentz forces are expected to change magnitude and direction locally due to increased electromagnetic activity close to the anode. This observation is also supported by previous measurements which show that helium produces a lower arc stagnation pressure than argon [27]. The predicted local decrease in flow vectors is validated by the lack of a strong horizontal jet parallel to the workpiece. Such a horizontal flow feature is characteristic of a higher velocity stream with increased momentum, as encountered in the argon visualisations, Fig. 3. Instead for helium, a 'bulb' shaped helium column rises up from the nozzle sides, mostly due to the difference in density with air. The black spots close to the arc in the 'hot' images are due to saturation of the CCD from excess arc radiation.

4.3. Alternating gases

As noted above, a 50% duty cycle was used for all alternating shielding gas tests, i.e. the argon and helium were switched on for equal times within the period of one shielding gas switching cycle. Fig. 5 shows the visualisation for a 10 l/m flow with alternating shielding gases within one cycle. Two switching frequencies are shown, 2 and 8 Hz, and the time of each image is indicated. In order to compare these two frequencies directly, the cycle period is indicated on the left-hand side of the figure: 0% and 100% of the cycle period correspond to the mid-point of the argon-dominated flow, while 50% corresponds to the mid-point of the helium-dominated flow. When using the alternating shielding gas technique, the shielding gas flow rapidly transitioned from one with the characteristics of pure argon, to one with the characteristics of helium. However, subtle differences were present as the mass fractions of each constituent varied, forming distinct, transient features over time.

The arc at 0% and 100% is typical of the argon flow of Fig. 3 and the arc at 50% is typical of the helium flow of Fig. 4. However, the arc in the 50% image at 8 Hz is brighter than at 2 Hz, suggesting that more argon was present. Ideally the mixture of the two gas flows exiting the nozzle would be equal at the two frequencies, but in practice the maximum fraction of helium comprising the arc during any given pulse was affected by flow and pre-flow conditions. The most significant contribution to this effect was the amount of premixing between the gases in the combined delivery pipe to the nozzle.

In order to characterise this pre-mixing, a theoretical analysis of axial dispersion in the gas line leading to the torch was conducted. It is assumed that the alternating cycle begins with a pulse of argon followed by a pulse of helium, both of equal lengths, flowing laminarly along the delivery pipe. The pipe has a circular cross-section with a solid inner core, i.e. the power supply to the welding torch. The mixing zone length L, is the length from the original argon–helium boundary to which the two gases are completely mixed, by the time the gas boundary reaches the end of the pipe and is delivered to the torch. It is determined by solving the diffusion equation, and is given by [28]:

$$L = 4\sqrt{Et}$$

where E is the dispersion coefficient and t is the total residence time of the boundary in the pipe. E for a laminar flow comprises contributions from both convection and diffusion, and can be calculated from a formula based on experiment and theory:

$$E = D + \frac{(d\,v)^2}{192D}$$

where d is the pipe's hydraulic diameter, v is the fluid's velocity and D is the binary gas diffusion coefficient which was calculated for argon and helium using the method of Fuller et al. [29]. The fluid velocity v can be calculated from the shielding gas volumetric flow rate and the pipe's hydraulic cross-section, assuming an incompressible flow. Therefore, the mixing zone length can be plotted against the shielding gas flow rate, as shown in Fig. 6. In the figure, the mixing zone length has been expressed as a percentage of the length of the original argon pulse. Hence a mixing length ratio of 100% indicates that the argon and helium pulses have completely mixed within the delivery pipe. Fig. 6 shows that the relative mixing of a pulse decreases as the flow rate increases.

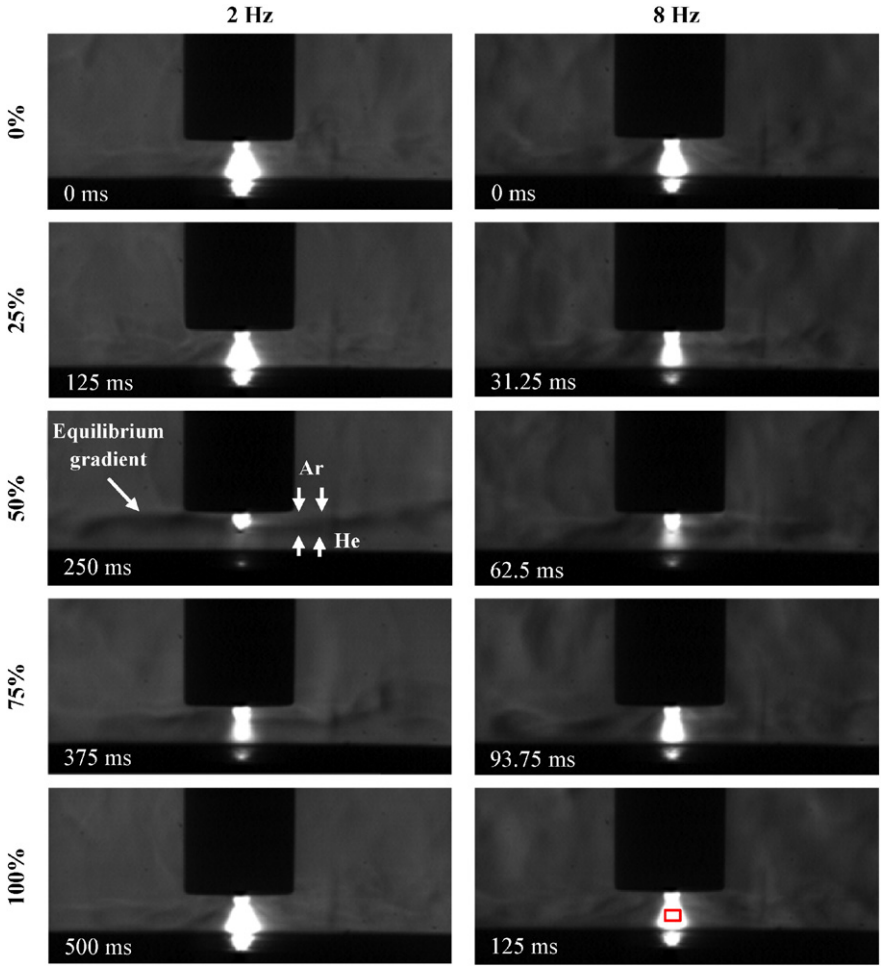

Fig. 5. Visualisation of 10 l/min flow with alternating shielding gases at different times within one shield gas switching cycle. 0% corresponds to argon dominated, 50% to helium dominated and 100% returning to argon dominated again. The typical arc radiation measurement area (see text) is shown in bottom right image.

Conversely, the relative mixing of a pulse increases as the alternating frequency increases.

Fig. 6 can be related to the previous images for the 10 l/min alternating shielding gas flow. For the 2 Hz alternating frequency, mixing occurs over approximately 15% of each argon pulse, while at 8 Hz it increases to approximately 60% as the duration of the gas pulses is four times smaller. The greater pre-mixing of the two shielding gas pulses at 8 Hz explains the brighter arc seen at 50% pulse position in Fig. 5. The dispersion calculation shows that for a 5 l/min shielding gas flow rate, pre-mixing is stronger than at 10 l/min: 30% ratio at 2 Hz and >100% at 8 Hz. The mixing ratio approximately doubles because the actual mixing zone length is similar in going from 10 to 5 l/min but the pulse length halves. A mixing length ratio of more than 100% of the argon pulse indicates that the pulses mix almost completely within the delivery pipe. These effects can be observed experimentally: Fig. 7 shows visualisations of the shielding gas alternating at 2 and 8 Hz for the 5 l/min flow rates. At 2 Hz the result is similar to Fig. 5, but at 8 Hz the arc intensity did not vary at different times through the 'pulse' cycle due to complete mixing of the two gases within the delivery pipe.

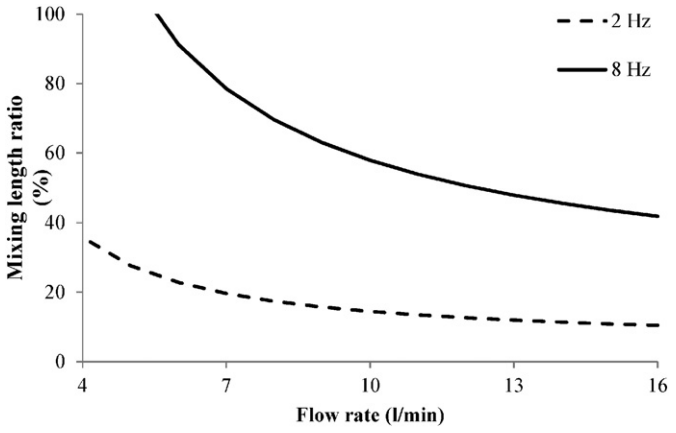

Fig. 6. Axial dispersion of a helium pulse within a 5 m GTAW gas delivery system. The gases will be mixed completely before reaching the torch if pulsed at high frequency and the flow rate is low.

In order to estimate the composition of the arc plasma at any instant, an estimate of the total arc radiative flux for the wavelengths of 633 ± 10 nm was made from the image sequences, for a 1 × 1.5 mm rectangular cross-sectional area below the cathode, indicated in Fig. 5. The emission characteristics already seen for pure argon and pure helium in Figs. 3 and 4 indicate that the brightest points correspond to an arc mainly comprised of argon, while the local minima in intensity correspond to an arc mainly comprised of helium.

Clearly the transition between these two arc types does not follow the square-wave with 50% duty cycle applied to the shielding gas switching valve. This is attributed to pre-mixing of the gases in the delivery pipe prior to the torch, in addition to turbulence in the weld region and transient flow vectors from electromagnetic field cycling. The extreme case is 5 l/min at 8 Hz where a constant arc intensity was

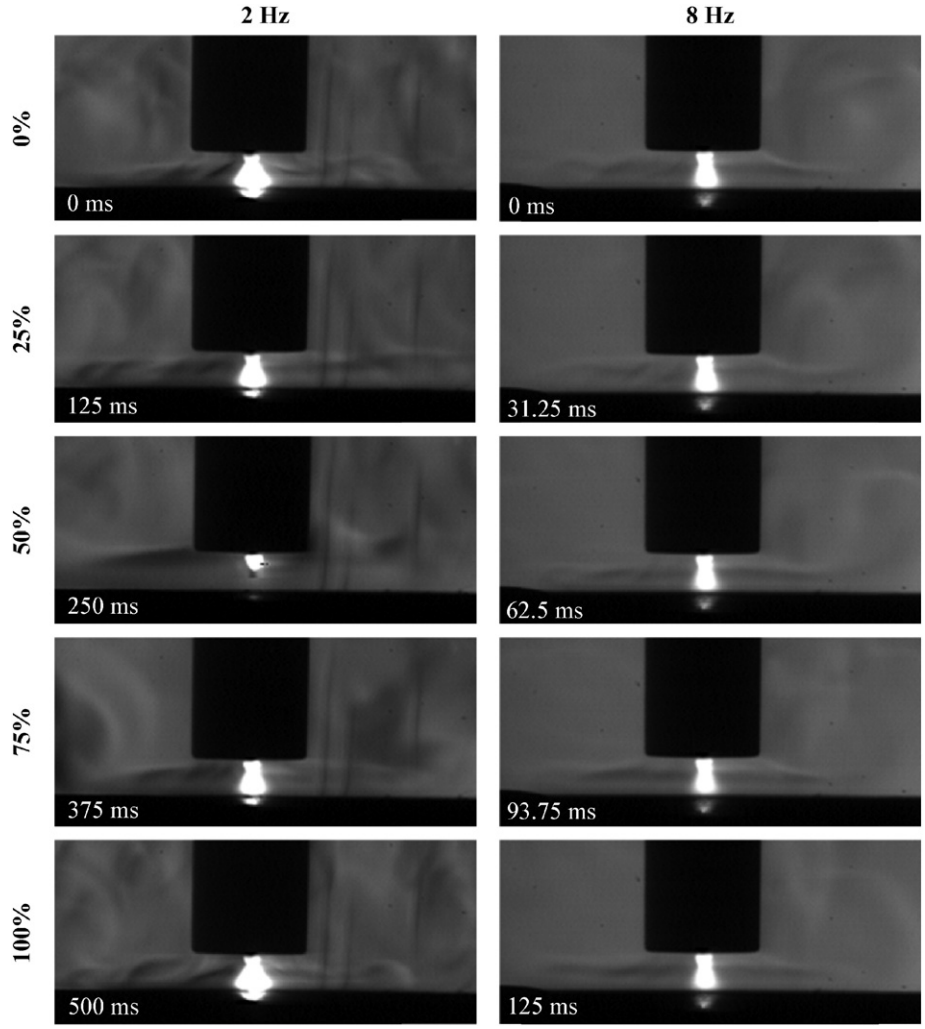

Fig. 7. Visualisation of 5 l/min flow with alternating gases at 2 and 8 Hz frequencies. The 2 Hz cycle shows transient arc characteristics, while for 8 Hz the process is almost steady state because the two gases have mixed fully in the delivery pipe.

observed in Fig. 7, due to the 100% pre-mixing of the shield gases prior to delivery. As discussed above, increasing the flow rate to 10 l/min at 8 Hz reduces pre-mixing to approximately 30%, although Fig. 8 shows that the time spent during each cycle at the minimum intensity is somewhat shorter than that. It could be observed from the associated video sequence of Fig. 5 that at 8 Hz the turbulence in the shielding gas flow reduced as helium entered the weld region, due to its lower viscosity. Indeed, during the helium pulse a horizontal intensity gradient (indicated in the figure) started to establish itself, but did not have sufficient time to form completely before the next argon pulse.

Fig. 8 shows lower minima when alternating at 2 Hz for both the 5 l/min and 10 l/min flows: overall a higher average fraction of helium exists in the arc due to reduced pre-mixing in the delivery pipe and the shielding gas has less vorticity due to the longer cycling times. Indeed, the associated video sequences of Figs. 5 and 7 at 2 Hz show the formation of a large horizontal density gradient extending from the top of the nozzle towards the edge of the image, indicating that equilibrium in gas concentration and partial pressures was reached during the helium pulse. This feature persisted throughout the helium phases, replacing the 'bulb' shaped buoyant plume observed in the steady state helium images, Fig. 4. The helium is restricted from flowing upwards, due to the heavier argon–air mixture acting to constrict it. The duration of the local minima in radiation intensity during the 2 Hz cycles shown in Fig. 8 was again somewhat less than the 50% duty cycle applied to the alternating shielding gas supply.

5. Discussion

The results presented in the previous section serve to characterise the flow at any given phase of the alternating shielding gas cycle. For the steady state flow during spot GTAW on a cooled copper plate, the argon flow was seen to be mildly turbulent with large eddies, whereas that of helium was smoother with buoyancy forces carrying the gas upwards to form a bulb shaped feature. When utilising the alternating shielding gas technique, the choice of pulsing frequency and flow rate determined the stability of a relatively stable horizontal region of helium shielding that formed in the weld region, maintained in position by the denser argon from the preceding pulse. It might be supposed that lower turbulence entrains less argon into the weld region and thus increases heat transfer into the workpiece, affecting weld size and penetration. In order to test this idea, GTAW welds were performed directly on to 6 mm thick, DH36 grade steel plate under the same conditions as the previous tests on the cooled copper plate.

The macrographs of the weld geometry produced for the shielding gas configurations used previously are shown in Fig. 9. As expected, the weld produced using pure helium resulted in a considerably larger weld size and penetration compared to the other shielding gas configurations. Due to 100% pre-mixing in the delivery pipe, the alternating flow at 5 l/min and 8 Hz provides a useful reference for a standard 50/50 (by volume) pre-mixed argon/helium shielding gas cylinder. Compared to this reference case, the weld width for the three cases where the

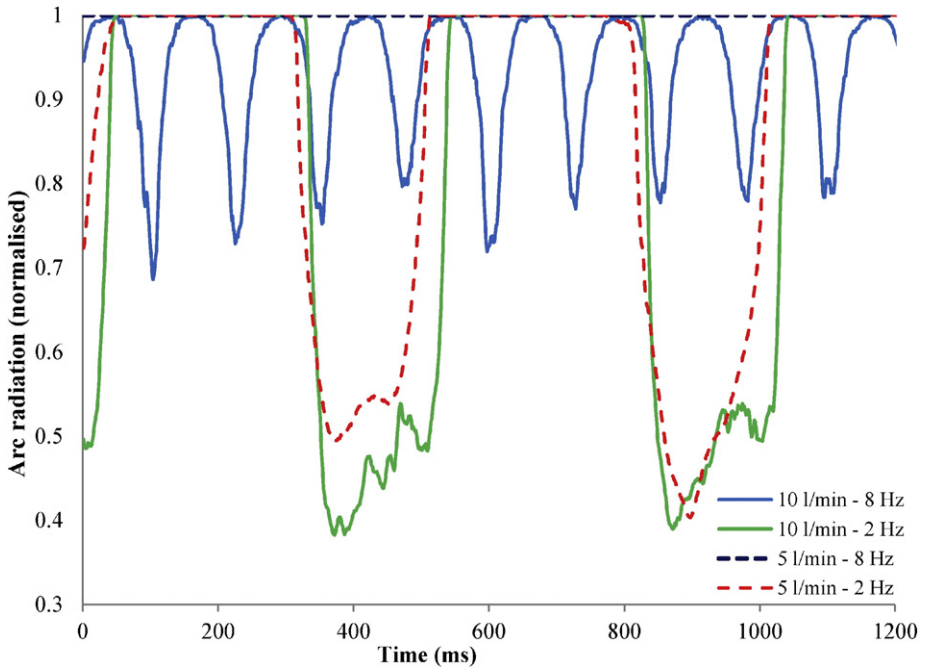

Fig. 8. Normalised arc radiation measurements obtained through image processing of the visualisations. The intensity of radiation is directly related with the fraction of ionised argon in the arc plasma, since helium emissions are much lower for the wavelengths allowed by the 633 nm band pass filter.

flow was alternated increased by 3% on average, while the depth of penetration increased by 13% on average. The welds made using the non-premixed flows were almost identical regardless of the flow rate used, establishing the 2 Hz, 5 l/min case as the most economical option.

The other important function of the shielding gas is to prevent porosity in the weld. The main mechanism for the entrainment of contaminants such as air or nitrogen from the environment into the weld is two-fold. Firstly, air mixes with the bulk flow through convection and diffusion. In the vicinity of the arc, the radial component of the flow is generally turned inwards and perpendicular to current's path in the plasma, accelerating gas from the secondary jet towards the electrode [23]. Consequently, the degree to which the secondary jet mixes with the surrounding air close to the nozzle predominantly dictates the extent of contamination in the weld.

Through inspection of the image sequences under flow rates of 5 and 10 l/min, it was found that the coverage area would be larger

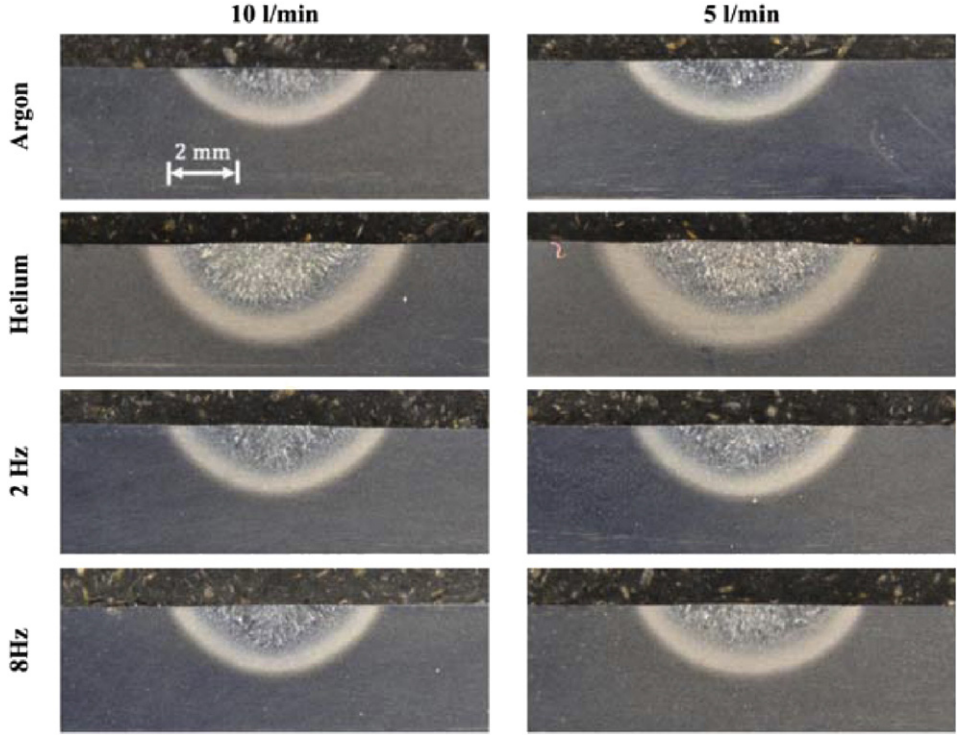

Fig. 9. Weld macrographs showing effect of shielding gas configuration. Due to pre-mixing, the alternating flow at 5 l/min and 8 Hz provides a useful reference for a standard 50/50 (by volume) pre-mixed argon/helium shielding gas cylinder.

than the weld pool regardless of the shielding gas composition or supply method, provided no cross draughts were present. With this condition satisfied, the gas would be expected to have shielded the weld adequately at all times in both cases. Still, these results are specific to the welding setup used, and the stand-off distance or indeed nozzle diameter would influence the degree of porosity or microporosity in the weld. At the same time, a general trend in gas behaviour was observed, which can be expected of most GTAW setups provided a reasonable combination of welding parameters are implemented.

Radiographic examination was performed on each experimental weld in order to detect discontinuities through the thickness of the weld. All the shielding gas configurations reported produced welds free from undesirable imperfections, which would pass industrial testing. The defect level, i.e. the percentage of the x-ray image that exhibited a shade in contrast to that of the bulk material, is used to characterise the level of micro-porosity, metallic and non-metallic inclusions. Its distribution was found to be consistent throughout the range of shielding gas parameters (composition and flow rate) investigated, and therefore all configurations produced welds in which the imperfections present would not be detrimental to the overall weld integrity.

6. Conclusions

This study visualised the flow of an alternating supply of argon and helium shielding gas during GTAW. In all cases, a 50% duty cycle between the two gases was applied, although in practice the duration of the arc associated with the helium pulse was less than the 50%, and more than 50% for the argon pulse, due to premixing between the gases in the combined delivery pipe to the nozzle and shield flow conditions after the nozzle. By choosing an appropriate pulsing frequency and flow rate, a stable horizontal region of helium was observed in the weld region, maintained in position by the denser argon from the preceding pulse. A 13% increase in weld penetration was observed with the alternating shielding gas method compared to the 'pre-mixed' case, suggesting that the helium is used more efficiently with the alternating shielding gas method. The understanding of this mechanism can be applied to other shielding gas mixtures and welding geometries in order to optimize performance.

Acknowledgements

This work was supported by the Engineering and Physical Sciences Research Council (Grant numbers EP/G037523/1 and EP/K030884/1) and BAE systems. Relevant research data present in this publication can be accessed at http://dx.doi.org/10.17861/209ad7ad-f274-43b7-acc0-1dc081aa4788.

Appendix A. Supplementary data

Supplementary data to this article can be found online at http://dx.doi.org/10.1016/j.matdes.2015.11.085.

References

[1] J. Cunningham, Pulsed Welding and Cutting by Variation of Composition of Shielding Gas, US3484575 A, 1969 (http://www.google.co.uk/patents/US3484575 accessed March 27, 2015).
[2] O.M. Novikov, A.S. Persidskii, E.P. Rad'ko, A.V. Baranovskii, B.A. Khasyanov, Effect of changes in the composition of the gas shielding medium on the properties of arc welded joints in aluminium alloys, Weld. Int. 27 (2013) 222–225, http://dx.doi.org/10.1080/09507116.2012.715891.
[3] B.Y. Kang, Y.K.D.V. Prasad, M.J. Kang, H.J. Kim, I.S. Kim, Characteristics of alternate supply of shielding gases in aluminum GMA welding, J. Mater. Process. Technol. 209 (2009) 4716–4721, http://dx.doi.org/10.1016/j.jmatprotec.2008.11.036.
[4] S.W. Campbell, A.M. Galloway, N.A. McPherson, A. Gillies, Evaluation of gas metal arc welding with alternating shielding gases for use on AA6082T6, Proc. Inst. Mech. Eng. B J. Eng. Manuf. 226 (2012) 992–1000, http://dx.doi.org/10.1177/0954405412439672.
[5] S. Campbell, A. Galloway, N. McPherson, Artificial neural network prediction of weld geometry performed using GMAW with alternating shielding gases, Weld. J. 91 (2012) 174S–181S.
[6] R.G. Tazetdinov, O.M. Novikov, A.S. Persidskii, B.A. Khasyanov, E.N. Ivanov, L.T. Plaksina, Arc welding in shielding gases with alternate pulsed supply of dissimilar gases, Weld. Int. 27 (2013) 311–314, http://dx.doi.org/10.1080/09507116.2012.715912.
[7] F.H. Ley, S.W. Campbell, A.M. Galloway, N.A. McPherson, Effect of shielding gas parameters on weld metal thermal properties in gas metal arc welding, Int. J. Adv. Manuf. Technol. 1–9 (2015), http://dx.doi.org/10.1007/s00170-015-7106-2.
[8] B.Y. Kang, Y.K.D.V. Prasad, M.J. Kang, H.J. Kim, I.S. Kim, The effect of alternate supply of shielding gases in austenite stainless steel GTA welding, J. Mater. Process. Technol. 209 (2009) 4722–4727, http://dx.doi.org/10.1016/j.jmatprotec.2008.11.035.
[9] A. Traidia, F. Roger, A computational investigation of different helium supplying methods for the improvement of GTA welding, J. Mater. Process. Technol. 211 (2011) 1553–1562, http://dx.doi.org/10.1016/j.jmatprotec.2011.04.008.
[10] S.W. Campbell, A.M. Galloway, N.A. McPherson, Techno-economic evaluation on the effects of alternating shielding gases for advanced joining processes, Proc. Inst. Mech. Eng. B J. Eng. Manuf. (2011), http://dx.doi.org/10.1177/0954405411408353 (0954405411408353).
[11] W.B. Moen, G.J. Gibson, Schlieren analysis of inert-gas arc shields, Weld. J. 31 (1952) 208–213.
[12] G.J. Gibson, Gas flow requirements for inert-gas shielded arc welding, Weld. J. 32 (1953) 128s–208s.
[13] T. Okada, H. Yamamoto, S. Harada, Observation of the shielding gas flow pattern during arcing by the use of a laser light source, Arc Phys. Weld Pool Behav. 1 (1980) 203–213.
[14] M. Schnick, M. Dreher, I.J. Zschetzsche, U. Füssel, A. Spille-Kohoff, Visualization and optimization of shielding gas flows in arc welding, Weld. World 56 (2012) 54–61.
[15] V. Beyer, S.W. Campbell, G.M. Ramsey, A.M. Galloway, A.J. Moore, N.A. McPherson, Systematic study of effect of cross-drafts and nozzle diameter on shield gas coverage in MIG welding, Sci. Technol. Weld. Join. 18 (2013) 652–660, http://dx.doi.org/10.1179/1362171813Y.0000000143.
[16] M. Dreher, U. Füssel, S. Rose, M. Häßler, M. Hertel, M. Schnick, Methods and results concerning the shielding gas flow in GMAW, Weld. World (2013), http://dx.doi.org/10.1007/s40194-013-0038-2.
[17] E. Siewert, G. Wilhelm, M. Häßler, J. Schein, T. Hanson, M. Schnick, et al., Visualization of gas flows in welding arcs by the schlieren measuring technique, Weld. J. 94 (2014) 1s–5s.
[18] H. Shardin, Toepler's schlieren method: basic principles for its use and quantitative evaluation, Forsch. Geb. Ingenieurwes. Ausg. B 5 (1934).
[19] G.S. Settles, Schlieren and Shadowgraph Techniques: Visualizing Phenomena in Transparent Media, Springer, 2001.
[20] D. Schwass, M. Wittlich, M. Schmitz, H. Siekmann, Emission of UV Radiation During arc Welding, Institute of Occupational Safety and Health of the German Social Accident Insurance (IFA), Sankt Augustin, 2011.
[21] L.M. Weinstein, Review and update of lens and grid schlieren and motion camera schlieren, Eur. Phys. J. Spec. Top. 182 (2010) 65–95, http://dx.doi.org/10.1140/epjst/e2010-01226-y.
[22] A.B. Murphy, M. Tanaka, K. Yamamoto, S. Tashiro, T. Sato, J.J. Lowke, Modelling of thermal plasmas for arc welding: the role of the shielding gas properties and of metal vapour, J. Phys. Appl. Phys. 42 (2009) 194006, http://dx.doi.org/10.1088/0022-3727/42/19/194006.
[23] J. Lancaster, The Physics of Welding, International Institute of Welding, 1986.
[24] D. Salem, R. Hannachi, Y. Cressault, P. Teulet, L. Béji, Radiative properties of argon–helium–nitrogen–carbon–cobalt–nickel plasmas used in CNT synthesis, J. Phys. Appl. Phys. 48 (2015) 065202, http://dx.doi.org/10.1088/0022-3727/48/6/065202.
[25] Z.H. Rao, S.M. Liao, H.L. Tsai, Effects of shielding gas compositions on arc plasma and metal transfer in gas metal arc welding, J. Appl. Phys. 107 (2010) 044902, http://dx.doi.org/10.1063/1.3291121.
[26] P.G. Jönsson, T.W. Eagar, J. Szekely, Heat and metal transfer in gas metal arc welding using argon and helium, Metall. Mater. Trans. B Process Metall. Mater. Process. Sci. 26 (1995) 383–395, http://dx.doi.org/10.1007/BF02660980.
[27] S.W. Campbell, A.M. Galloway, N.A. McPherson, Arc pressure and weld metal fluid flow while using alternating shielding gases. Part 1: arc pressure measurement, Sci. Technol. Weld. Join. 18 (2013) 591–596, http://dx.doi.org/10.1179/1362171813Y.0000000142.
[28] E.L. Cussler, Diffusion: Mass Transfer in Fluid Systems, Cambridge University Press, 1997.
[29] E.N. Fuller, P.D. Schettler, J.C. Giddings, New method for prediction of binary gas-phase diffusion coefficients, Ind. Eng. Chem. 58 (1966) 18–27.